Comparative study of the carbide-modified surfaces C/Mo(110) and C/Mo(100) using high-resolution x-ray photoelectron spectroscopy

Christoph Gleichweit,[1] Christian Neiss,[2] Sven Maisel,[2] Udo Bauer,[1] Florian Späth,[1] Oliver Höfert,[1] Florian Vollnhals,[1] Martin Drost,[1] Hubertus Marbach,[1] Andreas Görling,[2] Hans-Peter Steinrück,[1,3] and Christian Papp[1,*]

[1]*Lehrstuhl für Physikalische Chemie II, Friedrich-Alexander-Universität Erlangen-Nürnberg, Egerlandstrasse 3, 91058 Erlangen, Germany*

[2]*Lehrstuhl für Theoretische Chemie, Friedrich-Alexander-Universität Erlangen-Nürnberg, Egerlandstrasse 3, 91058 Erlangen, Germany*

[3]*Erlangen Catalysis Resource Center, Friedrich-Alexander-Universität Erlangen-Nürnberg, Egerlandstrasse 3, 91058 Erlangen, Germany*

(Received 12 May 2015; revised manuscript received 6 July 2015; published 22 July 2015)

The preparations of single (monolayer) and bulk carbides on the Mo(110) and Mo(100) single crystals are followed *in situ* at 1200 K using synchrotron-based high-resolution x-ray photoelectron spectroscopy of the C 1*s* and core Mo $3d_{5/2}$ levels. By comparing the experimental results to first principles calculations using density functional theory, we suggest real-space surface structures for the carbide-modified surfaces. For a monolayer carbide on Mo(110), carbon dimers adsorb in the long-bridge site, most likely at a coverage of 3/8 ML carbon atoms per Mo surface atom. For the bulk carbide, we find a coverage of ∼0.5 ML on the surface, and the calculations show that single carbon atoms are more stable than dimers on the surface. The monolayer carbide on Mo(100) exhibits a coverage of ∼1 ML and agrees with previous studies, while the bulk carbide preparation probably leads to a faceting of the surface.

DOI: 10.1103/PhysRevB.92.014114 PACS number(s): 82.80.Pv, 71.15.Mb, 81.05.Je

I. INTRODUCTION

Transition metal carbides (TMC) are known for the 4*d* and 5*d* elements of groups IV–V and for all 3*d* elements. They are produced by dissolving carbon in the corresponding transition metal. During that process, carbon is incorporated into interstitial sites of the metal lattice [1], which leads to changes in the physical and chemical properties of the resulting materials [2–4]. In many cases, both activity and selectivity in catalytic reactions are changed and/or the resistance to poisoning is increased [3]. In particular, early TMCs have attracted considerable attention due to similarities of their catalytic properties to those of the precious Pt-group metals (Pd, Ru, Rh) [5]. In fact, these similarities have been confirmed for a number of reactions, including hydrogenation, dehydrogenation, and hydrogenolysis of hydrocarbons [4,6], while, one the other hand, very different reaction pathways have been reported for oxygen-containing molecules, as summarized in a review of Stottlemyer *et al.* [7].

Experimental surface science studies of carbide surfaces in an ultrahigh vacuum (UHV) have been performed either on bulk carbide single crystals, carbide-modified metal single crystals, or polycrystalline carbide thin films. For instance, numerous investigations have been performed on the surfaces of bulk Mo_2C single crystals, e.g., by neutron diffraction [8,9], scanning tunneling microscopy (STM) [10–12], and density functional theory (DFT) calculations [13–20] (for more details, see Ref. [4]). However, the advantage of carbide-modified metal single crystals is that the amount of carbon dissolved in the crystal can be tuned from zero up to the stoichiometric amount of the corresponding bulk carbide. The disadvantages are uncertainties concerning the exact surface structure of such surface carbide layers, as these tend to display imperfect terminations, defects [4], and, in some cases, surface reconstructions [21,22].

Among the group VI metals, thin molybdenum and tungsten carbide layers have been investigated extensively [3,4]. These carbides are prepared by providing carbon at elevated temperatures. This is mostly done by exposing the surface to unsaturated hydrocarbons such as ethylene, typically at ∼900 K to crack the molecules, and result in a carbon layer on the surface [22,23]. By annealing to temperatures above 1100 K, carbon diffusion to the bulk occurs, i.e., the excess carbon from the surface is driven into interstitial sites, and a phase with the preferred stoichiometry is formed (e.g., Mo_2C, W_2C, WC) [3,24–26]. Alternatively, it has been shown that exposing the crystal to, e.g., ethylene, above the temperature for diffusion is sufficient for carburization [22], and simply heating a carbon-containing crystal can also lead to formation of surface carbide layers by diffusion from the bulk [27].

This paper focuses on the preparation and comparison of carbide-modified Mo(100) and Mo(110) single crystal surfaces. The most important current findings are summarized below. The carbide overlayer on Mo(110) has been characterized thoroughly [4], including a STM paper, by Yu *et al.* [28]. These authors reported three low energy electron diffraction (LEED) patterns when increasing the ethylene exposure from 2 up to 9 Langmuir (L); the pattern at the largest exposure corresponded to the $p(4 \times 4)$-structure, in line with literature [26,29,30]. Combining STM and LEED, they proposed a real-space structure with a coverage with one carbon atom at a hollow site per (4×4)-unit cell, which is a coverage of $1/16 = 0.0625$ ML [28]. In their analysis, the authors assigned protrusions in their STM images to the adsorbed carbon atoms despite the fact that carbon was reported to appear as a depression in earlier STM papers on the (001) surface of orthorhombic bulk Mo_2C [10,11]. They attribute this different appearance to a possible contrast inversion by adsorbed carbon at the STM tip. From Auger electron spectroscopy (AES), Frühberger and Chen reported a C/Mo-ratio approaching 0.45 at higher ethylene dosages, indicating that significant carburization also occurs in deeper layers within the AES sampling depth [26]. It is important to note here that thicker carbide layers also exhibit

*Corresponding author: christian.papp@fau.de

a $p(4 \times 4)$ LEED pattern, though with increased background intensity [26,31]. From near-edge x-ray absorption fine structure (NEXAFS) studies at the K-edge of C/Mo(110), it was deduced that the $p(4 \times 4)$-C/Mo(110) surface has a similar termination as the C-terminated (001) surface of bulk orthorhombic Mo_2C with a nominal coverage of 0.5 ML [4,12,32,33]. Furthermore, a (4×4) structure found in LEED by Clair *et al.* [10] for C-terminated bulk orthorhombic $Mo_2C(001)$ was assigned to three (2×1) orthorhombic domains rotated by 120° (observed in STM), leading to a coverage of $3/8 = 0.375$ ML. Considering the great similarity to the results of Clair *et al.*, the coverage of 0.0625 ML deduced by Yu *et al.* [28] seems questionable.

In comparison, the Mo(100) surface is much less explored, and in particular no STM study was reported. By LEED, Guillot *et al.* [27] found several LEED patterns when increasing the coverage from the clean surface up to saturated Mo_2C. At very low carbon coverages, a $p(4 \times 4)$ pattern appeared, followed by a $c(2 \times 2)$ pattern at 0.5 ML, a $c(6 \times 2)$ pattern at higher coverages, and finally a $p(1 \times 1)$ pattern at saturation of 1.0 ML [27,34]. For the $c(2 \times 2)$ structure, Jentz *et al.* [35] performed a tensor LEED study and found that carbon occupies every second fourfold hollow site of the Mo(100) surface, with the molybdenum atoms below that hollow site being slightly buckled. The exact same $c(2 \times 2)$ structure was found in a LEED I(V) study of the $Mo_{0.75}Re_{0.25}(100)$ alloy surface by Kottcke *et al.* [36]. The authors argued that adsorbate interactions induce segregation of Mo to the topmost layer, resulting in the same structure as for pure Mo(100). Notably, Mo and Re exhibit only a negligible difference in size, and thus no lattice strain is induced. At higher carbon concentrations, a $p(1 \times 1)$ structure with all carbon atoms in the fourfold hollow sites is found for the $Mo_{0.75}Re_{0.25}(100)$ alloy [36]. Interestingly, a $p(1 \times 1)$ LEED structure is found also for a thicker carbide consisting of two layers, which leads to a model for the layer-wise growth of such carbides: the carbide formation in the first layer leads to an expansion of the first to second layer distance, which also enlarges the octahedral interstitial sites between the layers. During growth of the second carbide layer, these sites are occupied by additional carbon atoms. From these considerations, we conclude that in the $p(1 \times 1)$−C/Mo(100) system, all fourfold hollow sites are occupied by carbon atoms, as suggested also in other studies [37,38].

Herein, we present a comparative study of the carburization of the Mo(100) and Mo(110) surfaces and the properties of the corresponding surface and bulk carbides. Using synchrotron-based high-resolution x-ray photoelectron spectroscopy (HR-XPS), we aim at elucidating the spectroscopic differences and similarities of the two crystal facets. Carbide formation by exposure to ethylene and subsequent oxidative carbon removal was followed by quantitative analysis of the C 1*s*, Mo 3*d*, and O 1*s* core levels. We show that monolayer carbides can be prepared on both crystal facets and that bulk carbides can be formed by additional carburization of the underlying layers and the bulk Mo. To elucidate the surface carbides in more detail, first principles calculations using DFT were performed and related to the experimental data. By combining the DFT results with the experimental data, we propose a structure for the surface carbides, including a suggestion for an alternative structure of the carbide overlayer on Mo(110), which are in better agreement with experimental findings than earlier structure proposals.

II. RESULTS AND DISCUSSION

A. Monolayer carbide preparation and oxidative removal on Mo(110)

To begin, we discuss the preparation of a single carbide layer on Mo(110), which is denoted as monolayer carbide. We monitored the transformation from a partly oxygen-covered (∼0.5 ML) surface to the carbide *in situ* by continuously measuring the C 1*s* and Mo $3d_{5/2}$ core levels while exposing the surface to ethylene at 1200 K. The photon energy was set to 380 eV, which results in a high surface sensitivity due to the low kinetic energy of about 100 and 150 eV for emission from the C 1*s* and Mo $3d_{5/2}$ levels, respectively. In addition, separate experiments were performed with 650 eV photon energy in order to study the O 1*s* region and the C 1*s* region with increased bulk sensitivity due to the higher kinetic energy; see Supplemental Material (Figs. S1–S4) [39] for these experiments.

Figure 1 shows selected x-ray photoelectron (XP) spectra in the Mo $3d_{5/2}$ (a) and C 1*s* (b) regions at different exposures of ethylene at 1200 K; note that since the two regions have been measured alternately, the denoted exposures are not identical. The spectra at 0 Langmuir (L) show the situation on the surface at the starting point of the experiment, where no carbon signal is observed in the C 1*s* region. In the Mo $3d_{5/2}$ region, we find the peak due to the Mo bulk at a binding energy of 227.95 eV and two peaks at 227.87 and 228.16 eV that are related to adsorbed oxygen, which remained

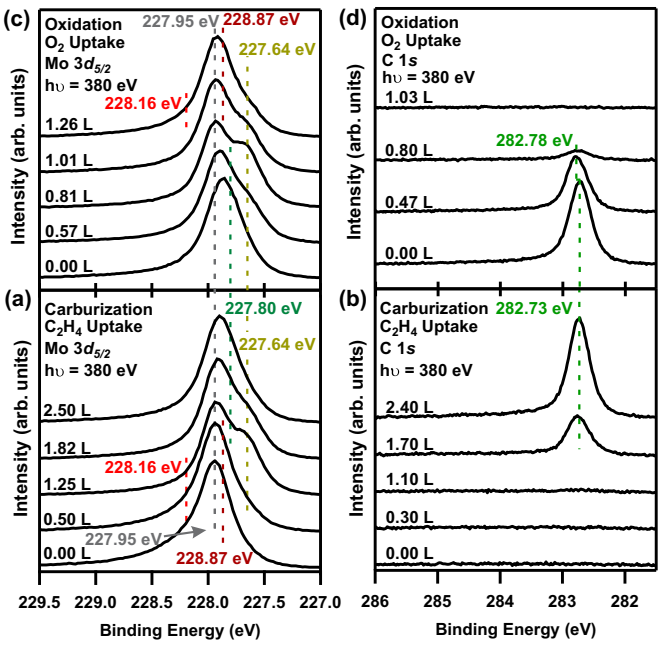

FIG. 1. (Color online) Selected XP spectra of the monolayer carbide preparation on Mo(110) at different doses of ethylene both in the (a) Mo $3d_{5/2}$ and the (b) C 1*s* core levels. (c), (d) Respective spectra of the subsequent oxidation are presented ($T_S = 1200$ K, $h\nu = 380$ eV).

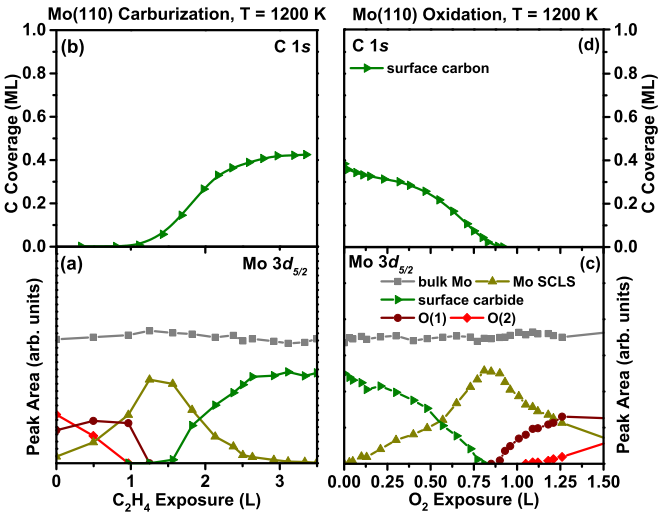

FIG. 2. (Color online) Quantitative analysis of the monolayer carbide preparation on Mo(110) both in the (a) Mo $3d_{5/2}$ and (b) the C 1s core levels. (c), (d) Analysis of the subsequent oxidation is presented ($T_S = 1200\,\mathrm{K}$, $h\nu = 380\,\mathrm{eV}$).

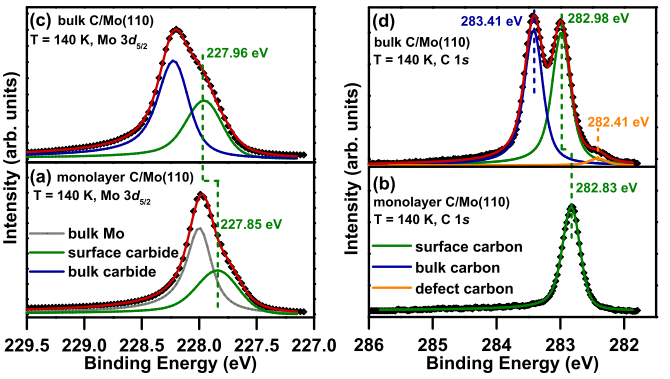

FIG. 3. (Color online) Comparison between the monolayer (a) and (b) and bulk (c) and (d) carbide overlayers of C/Mo(110) at low temperatures for the (a) and (c) Mo $3d_{5/2}$ core level and (b) and (d) C 1s core level ($T = 140\,\mathrm{K}$, $h\nu = 380\,\mathrm{eV}$).

on the Mo(110) surface after the oxidative removal of carbon by exposure to oxygen; the denoted peak energies are deduced by fitting the peaks, with the fitted spectra shown in Fig. S5 in the Supplemental Material [39]. When exposing the surface to 1.4×10^{-8} mbar ethylene, which instantaneously reacts at 1200 K, the oxygen-induced peaks decrease, see, e.g., the spectrum at 0.5 L in the Mo $3d_{5/2}$ region. Simultaneously, a new peak appears at 227.64 eV and reaches maximum intensity at $\sim$1.5 L, when the oxygen-derived peaks have completely vanished. It is shifted by -0.31 ± 0.01 eV with respect to the Mo bulk peak, in very good agreement with the reported surface core level shift (SCLS) of -0.33 eV for the surface atoms on the clean Mo(110) surface [40]. It will thus be denoted as Mo SCLS peak in the following, and its intensity is a measure of the number of Mo surface atoms that are not in direct contact to adsorbates (oxygen or carbon). By fitting the spectra with different components, we determined the contributions of the different Mo peaks, as shown in Fig. 2(a). Between 0 to $\sim$1.5 L, the oxygen-derived Mo peaks [denoted as O(1) and O(2), red] decrease, and simultaneously the Mo SCLS peak (ochre) increases.

As soon as the oxygen-derived Mo peaks vanish, a sharp, asymmetric peak develops in the C 1s region at 282.73 eV; see spectrum at 1.7 L in Fig. 1(b). During this transition from a partly oxygen-covered (and carbon-free) to a carbon-covered (and oxygen-free) surface, the crystal must have been almost clean at some point; the Mo $3d_{5/2}$ spectrum at 1.25 L is considered representative of the pristine Mo(110) surface. When all oxygen is removed at this exposure, the actual carburization starts. Using quadrupole mass spectrometry (QMS), desorption of CO is indeed observed and then vanishes after the complete removal of oxygen from the surface (data not shown). Please note that, as expected, CO is not observed on the surface at 1200 K.

As the C 1s signal rises, the Mo SCLS peak decreases. Furthermore, the spectrum at 2.50 L in Fig. 1(a) reveals that the Mo bulk peak shifts slightly to lower binding energies by -0.06 eV (to 227.89 eV) and increases in intensity. This indicates that this peak not only contains the Mo bulk contribution but also intensity from the monolayer carbide. In our peak fitting, we account for this fact by keeping the bulk contribution constant in intensity and position while introducing a new broad component at 227.80 eV; this monolayer carbide peak [green in Fig. 2(a)] accounts for all Mo surface atoms, i.e., in contact and not in contact with carbon, because we cannot distinguish these contributions experimentally. Up to 3.5 L, the monolayer carbide peak saturates, and the Mo SCLS vanishes. This saturation behavior could be due to two effects: Either sticking and dissociation of the ethylene molecule is prevented by the carbide layer, or, after dissociation, excess carbon diffuses into the bulk beyond the information depth of our measurements. Notably, the results for the preparation of the bulk carbide presented below strongly hint at diffusion into the bulk.

To further discuss the peak assignments, Figs. 3(a) and 3(b) show spectra of the monolayer carbide at low temperature, that is, $T = 140\,\mathrm{K}$. For this layer, we obtain a sharp $p(4 \times 4)$ pattern in LEED, as reported previously for a "thin" carbide [26]. Note that the XPS peaks show slightly different positions and are narrower as compared to the spectra taken at 1200 K, which is attributed to the applied heating current and/or thermal broadening at the elevated temperature. In the C 1s region, the monolayer carbide peak is found at 282.83 eV, while in the Mo $3d_{5/2}$ region, the Mo bulk peak is found at 228.00 eV and the monolayer carbide peak at 227.85 eV. To further support our peak assignments, we measured Mo $3d_{5/2}$ spectra at different photon energies, at $T < 140\,\mathrm{K}$. The resulting different kinetic energies of the electrons lead to changes in the inelastic mean free path (IMFP). Figure 4 shows the relative intensities of Mo bulk peak and the monolayer carbide peak versus kinetic energy (spectra shown in Fig. S6 [39]). As expected, the peak of the monolayer carbide decreases because it originates only from the topmost layer, and the Mo bulk peak increases with increasing kinetic energy due to the increased IMPF and probing depth at higher photon energies.

The quantitative nature of XPS allows us to determine the carbon coverage on the surface. From the spectrum of the saturated monolayer carbide in Fig. 3(b), we deduce a carbon coverage 0.43 ± 0.06 ML. This value contradicts the value

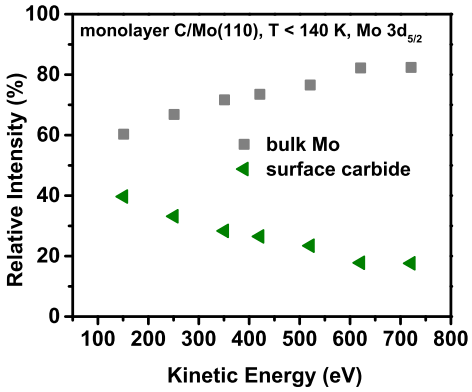

FIG. 4. (Color online) Relative peak ratios in the Mo $3d_{5/2}$ core level of the monolayer carbide on Mo(110) for different kinetic energies of the photoelectrons.

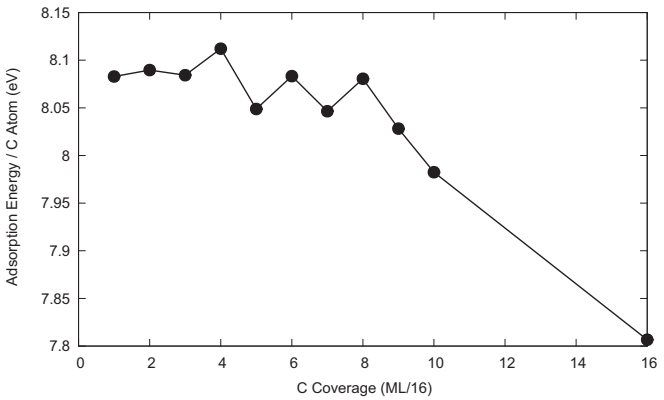

FIG. 6. Calculated adsorption energies per carbon atom for different coverages on Mo(110).

of 0.0625 ML proposed by Yu *et al.* [28] from STM (see the Introduction). We speculate that these authors erroneously assumed a contrast inversion; without that assumption, their surface coverage would nominally be 0.4375 ML, in line with our results.

In addition, as already mentioned, Clair *et al.* [10] noticed that the (4 × 4) LEED image can be explained by rectangular domains rotated by 120°, leading to a surface coverage of 3/8 ML (=0.375 ML), which is much more consistent with our findings. Based on these considerations, in our calculations the first guess for the positions of the adsorbed surface carbon atoms was based on a rectangular unit cell containing eight Mo surface atoms and three adsorbed carbon atoms, resulting in a coverage of 3/8 ML. By performing geometry optimizations starting from different configurations, we were able to find a number of structures representing local energy minima (see Fig. S7 [39]). Two distinct types of structures were found: one with only isolated carbon atoms and one with one singly adsorbed carbon atom and one carbon dimer (C-C bond length: 1.37 Å). The energetically lowest structure of each type is shown in Fig. 5. The adsorption geometry with the carbon

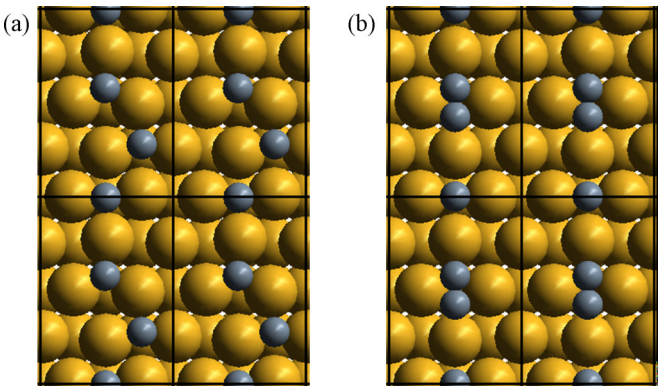

FIG. 5. (Color online) DFT optimized structures of monolayer C/Mo(110) with 3/8 ML coverage based on an orthorhombic unit cell (C atoms are depicted as gray, Mo atoms as gold), which gave the lowest energies in case of adsorption of three isolated carbon atoms and of a carbon dimer together with one isolated carbon atom, respectively.

dimer is more stable by 0.50 eV per carbon atom. This means that the formation of carbon dimers is strongly favored on Mo(110), and the presence of unpaired carbon atoms seems unlikely under the experimental conditions. To the best of our knowledge, such a dimerization of carbon on metallic surfaces has not been reported up to now and may be a peculiarity of the Mo(110) or, more general, the bcc(110) surface (see the next section). The calculated core level binding energies for adsorbed single carbon atoms and for carbon atoms of a carbon dimer differ by 1.17 eV (with the single carbon atom having the lower binding energy), but in the experimental XPS spectrum only one carbon species is found, see Figs. 1(b) and 3(b). These results prompted us to investigate other possible structures based on a (4 × 4) supercell of Mo(110), which is also found by the STM measured by Yu *et al.* [28]. To that end, we investigated carbon coverages from 1/16 ML [one carbon atom per (4 × 4) unit cell] up to 1 ML [16 carbon atoms per (4 × 4) unit cell]. For most coverages, different structures representing local energetic minima were found (see Figs. S8–S10 [39]). Again, structures with a maximal number of carbon dimers are the energetically lowest ones, whereas increasing numbers of adsorbed single atoms lead to a rising energy of the structures. In Fig. 6, the calculated adsorption energy per carbon atom for the energetically most favorable structures between coverages from 1/16 to 1 ML is shown. The favorable formation of carbon dimers is clearly indicated by the alternating behavior of the adsorption energies up to 0.5 ML with maxima at even numbers of carbon atoms in the unit cell. For coverages higher than 0.5 ML, adsorption energies become significantly smaller, suggesting saturation of the surface. Coverages of 3/8, 7/16, and 1/2 ML lie in the range of the experimentally determined coverage and are discussed further in more detail by calculating the core level binding energies for Mo and C and predicting STM images.

For the clean Mo(110) surface, we find a theoretical Mo SCLS of −0.46 eV, as compared to the experimental value of −0.31 eV, indicating that our computational method tends to overestimate core level shifts but gives the correct trend. For the energetically most favorable structure at 3/8 ML, one can distinguish two different types of surface Mo atoms: those that are in contact with a C dimer and those that are not (see Fig. 7). For the latter, a SCLS of −0.44 eV is calculated, which is

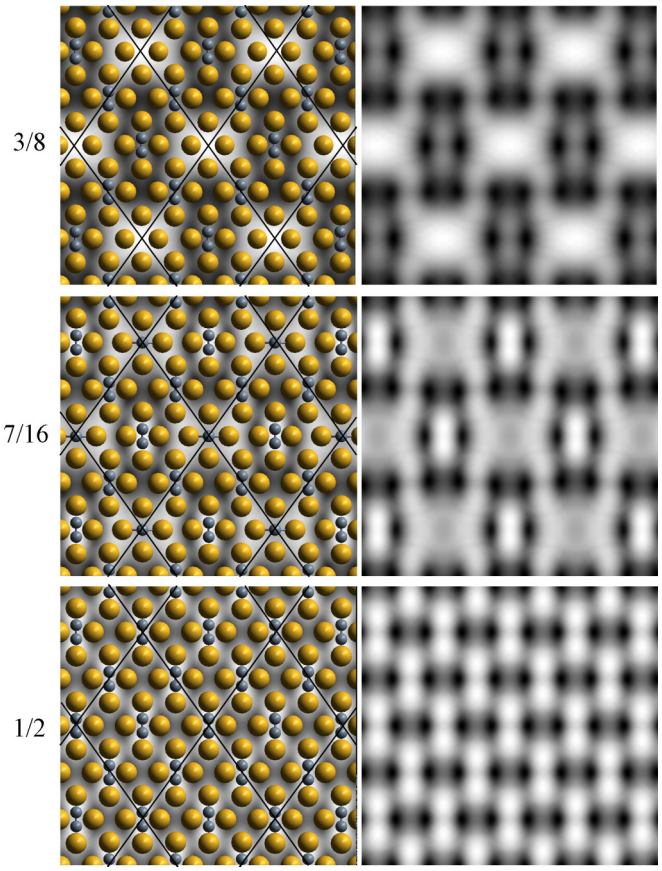

FIG. 7. (Color online) Calculated constant current STM images of the energetically most favorable structures for monolayer C/Mo(110) with different coverages (in ML). The $p(4 \times 4)$ unit cell is indicated by black lines. (Left panel) STM image overlayered with the surface structure; only the topmost Mo layer is indicated, (right panel) only STM. Isodensity surfaces of 3.3×10^{-7} atomic units are shown to simulate the STM images within the Tersoff-Hamann approach. Coloring as in Fig. 5.

practically identical to the SCLS of the clean Mo(110) surface, whereas the Mo atoms in contact to carbon dimers exhibit a smaller shift of -0.24 ± 0.02 eV. In the case of 1/2 ML coverage, all surface Mo atoms are in contact with carbon dimers, and a SCLS of -0.23 ± 0.04 eV is calculated. We note, however, that a coverage of 1/2 ML leads to an effectively smaller [namely a (2×2)] unit cell (see Fig. 7).

Thus, Mo surface atoms in the neighborhood of carbon dimers have a smaller SCLS than those of a clean Mo(110) surface, in agreement with the assignment of the experimental data. Comparing the 3/8 and 1/2 ML coverages, the core level binding energies of the carbon atoms are identical to within 0.01 eV.

For the 7/16 ML (=0.4375 ML) structure, the calculated Mo core level shifts indicate that the single carbon atom on the surface leads, on the one hand, to a significant broadening of the SCLSs of Mo surface atoms (we find a SCLS of -0.26 ± 0.08 eV of Mo next to a carbon dimer and -0.43 ± 0.12 eV for Mo next to a single carbon atom), and, as already observed for the rectangular cell, the core level binding energy of the singly attached carbon atom strongly deviates from the other carbon atoms in dimers (here by -0.77 eV). Since we have no experimental indication for two different carbon species and, as already discussed before, there is a thermodynamic driving force for the formation of carbon dimers, we think that structures with singly adsorbed carbon atoms on Mo(110) are unlikely.

In addition, simulated STM images are compared in Fig. 7. According to Yu *et al.* [28], the constant current STM image of single-layer carbon on Mo(110) exhibits protrusions consistent with four times the lattice constant of Mo(110). The calculated STM images of 3/8 and 7/16 ML C/Mo(110) reproduce the experimentally found image, whereas the image of 1/2 ML C/Mo(110) clearly shows the (2×2) super cell. As the 7/16 ML coverage has been ruled out (see above), the 3/8 ML covered structure seems most reasonable. Thus, our results suggest that the (4×4) LEED and STM images are generated by formation of carbon dimers on the Mo(110) surface. In passing, we note that also some other coverages yield similar STM images according to our calculations (see Figs. S8–S10 [39]) but are unlikely due to the experimentally determined carbon coverage.

Next, we follow the reverse process to the carburization, that is, the oxidation of the carbide at 1200 K by dosing O_2 at 4.6×10^{-9} mbar. The end point of the carburization experiment at 3.3 L C_2H_4 exposure in Figs. 2(a) and 2(b) is the starting point of the oxidation experiment, in Figs. 2(c) and 2(d) at 0 L O_2 exposure. Figure 1(c) shows selected Mo $3d_{5/2}$ spectra and Fig. 1(d) the respective C 1*s* spectra at different doses of oxygen. During the removal of the carbide, we identify two regimes: up to O_2 exposures of 0.5 L, we observe a slow, continuous decrease of the C 1*s* signal in Figs. 1(d) and 2(d). This behavior is attributed to the removal of carbon directly from the surface, which is partly replaced by carbon diffusing from the bulk to the surface. Simultaneously, in the Mo $3d_{5/2}$ region, a slow decrease of the monolayer carbide peak at 227.80 eV and an increase of the Mo SCLS peak at 227.64 eV occur. Above 0.5 L, the decrease of the C 1*s* peak accelerates until it vanishes around 0.9 L, which is attributed to a depletion of carbon in the bulk and a rapid removal of the monolayer carbide. In the Mo $3d_{5/2}$ region, the Mo SCLS peak at 227.64 eV also increases faster above 0.5 L. At 0.85 L, the onset of the oxygen-induced Mo signal at 227.87 eV is observed in the Mo $3d_{5/2}$ region, followed by a second oxygen-induced Mo contribution at 228.16 eV above 1.0 L, leading to a situation comparable to that before the carburization experiment. As we are not particularly interested in the surface oxide, we stop our discussion at this point. We conclude that at 1200 K, the removal of the monolayer carbide on the surface by oxidation is effectively the reverse process to the carburization using ethylene.

B. Bulk carbide preparation and oxidation on Mo(110)

The preparation of the monolayer carbide was performed at low ethylene pressures ($<10^{-7}$ mbar). It turns out that on Mo(110), a Mo_2C bulk carbide can be prepared at 1200 K by increasing the exposure by orders of magnitude. To achieve such high exposures, we exposed the sample to pressures in the 10^{-6} mbar regime. Note that as an alternative route also cycles of dosing ethylene at 900 K followed by flashes to above

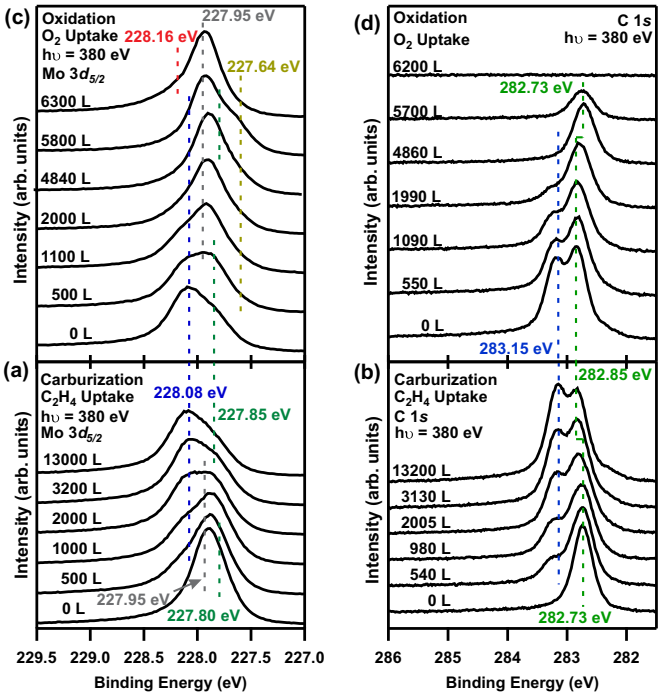

FIG. 8. (Color online) Selected XP spectra of the bulk carbide preparation on Mo(110) at different doses of ethylene both in the (a) Mo $3d_{5/2}$ and the (b) C 1*s* core levels. (c), (d) Respective spectra of the subsequent oxidation are presented ($T_S = 1200\,\mathrm{K}$, $h\nu = 380\,\mathrm{eV}$).

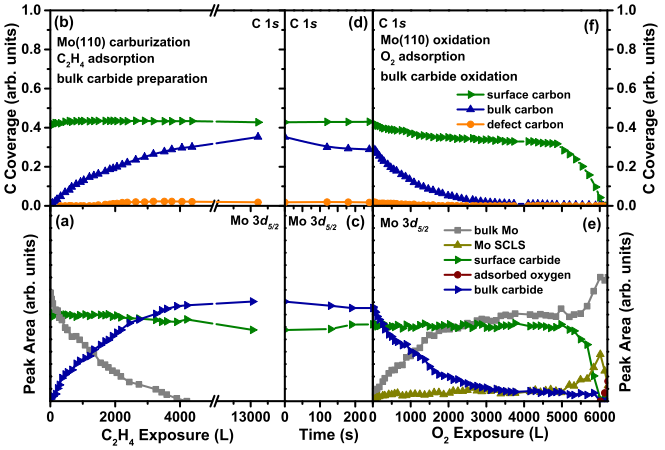

FIG. 9. (Color online) Quantitative analysis of the bulk carbide preparation of Mo(110) for both the (a) Mo $3d_{5/2}$ and (b) C 1*s* core levels. (e), (f) Respective data of the oxidation experiment is presented. Between the two experiments (c) and (d), the surface was monitored without dosing for 300 s ($T_S = 1200\,\mathrm{K}$, $h\nu = 380\,\mathrm{eV}$).

1200 K leads to formation of this bulk carbide [26]. However, we consider the isothermal carburization at 1200 K to be more suitable to study the system.

The starting point is the situation we find after the preparation of the monolayer carbide. Therefore, the spectra at 0 L in Figs. 8(a) and 8(b) are identical to those observed for the monolayer carbide at 3.5 L. In the C 1*s* region, we find one peak at 282.73 eV [Fig. 8(b)], whereas in the Mo $3d_{5/2}$ region [Fig. 8(a)], the Mo bulk peak at 227.95 eV and the monolayer carbide peak at 227.80 eV are observed. This surface was then first exposed to 1.8×10^{-6} mbar of ethylene using the supersonic molecular beam, and after 180 s (that is, ~270 L), the pressure was further increased to 3.2×10^{-6} mbar. At ~500 L, additional species are visible in the C 1*s* region at 283.15 eV and in the Mo $3d_{5/2}$ region at 228.08 eV, which we assign to bulk Mo_2C. With increasing exposure in the C 1*s* region, the bulk peak approaches the height of the surface peak at the end of our carburization experiment at 13200 L; at the same time, the surface peak continuously shifts to higher binding energies, ending at 282.85 eV. Simultaneously, in the Mo $3d_{5/2}$ region, the bulk Mo_2C peak at 228.08 eV increases, while the bulk Mo peak at 227.95 eV vanishes, and the surface carbide peak at 227.80 eV slightly shifts to higher binding energy (227.85 eV). Note that surface carbide is here understood as the topmost layer; at the beginning of the bulk carbide formation, this is the monolayer carbide (on top of Mo bulk), and at the end this is the surface layer of the bulk carbide. In both cases, similar binding energies are observed (the transition between the two cases is reflected by the shift to a higher binding energy).

Figures 9(a) and 9(b) show the quantitative analysis of the experiment. While the monolayer carbide is formed already after ~3 L exposure (see Fig. 2), the bulk carbide requires considerably larger exposures and is not saturated even after 13000 L [Fig. 9(a)]. This is attributed to diffusion of excess carbon deep into the bulk, that is, beyond the information depth of XPS. Only after the bulk in the surface-near-region is saturated with carbon, the Mo_2C bulk layers within the XPS information depth are populated up to saturation stoichiometry of Mo:C = 2:1. In the Mo $3d_{5/2}$ region during carburization, the Mo bulk peak vanishes, and the intensity from the carbide surface shows no significant changes.

Further support for the proposed carbon diffusion into the bulk comes from Figs. 9(c) and 9(d), which shows the peak intensities for 300 s after closing the molecular beam: The Mo_2C bulk signals decrease in both the C 1*s* and Mo $3d_{5/2}$ regions, and the Mo $3d_{5/2}$ surface carbide peak slightly increases. Since desorption of elemental carbon is not expected, this is a strong indication for the diffusion of carbon from near the surface to beyond our information depth.

In Figs. 3(c) and 3(d), the C 1*s* and Mo $3d_{5/2}$ spectra of the Mo_2C bulk carbide at 140 K are shown, respectively, in comparison to the monolayer carbide. In the C 1*s* region of the bulk Mo_2C [Fig. 3(d)], the bulk contribution is found at 283.41 eV and that of the surface layer at 282.98 eV. The small binding energy differences as compared to Fig. 8 are again attributed to the applied heating current and/or thermal broadening at the elevated temperature. The additional small signal at ~282.41 eV in Fig. 3(d) varies slightly in intensity and position for different preparations and is assigned to surface defects of the bulk carbide. Note that while the $p(4 \times 4)$ LEED pattern is very sharp for the monolayer carbide, it appears weaker and more diffuse, with an increased background intensity, for the bulk carbide. The comparison of the Mo $3d_{5/2}$ region of the bulk carbide in Fig. 3(c) to the monolayer carbide in Fig. 3(a) shows that both carbides exhibit a surface carbide peak due to carbon-coordinated Mo surface atoms. The peak position slightly differs, with a binding energy of

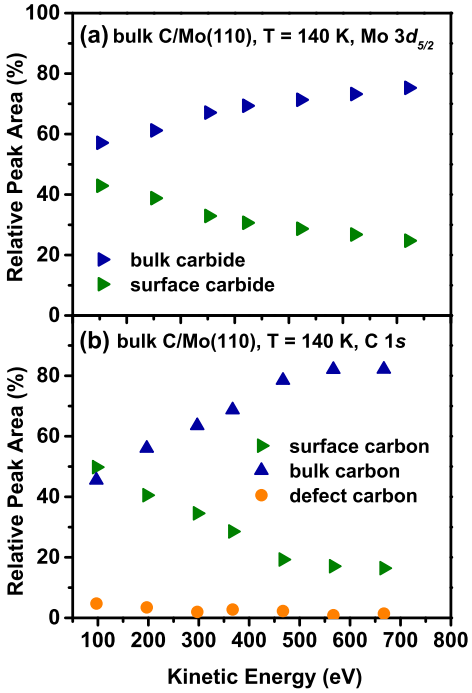

FIG. 10. (Color online) Relative peak ratios of the bulk carbide on Mo(110) for different kinetic energies of the photoelectrons in the (a) Mo $3d_{5/2}$ and (b) C 1s core levels, respectively.

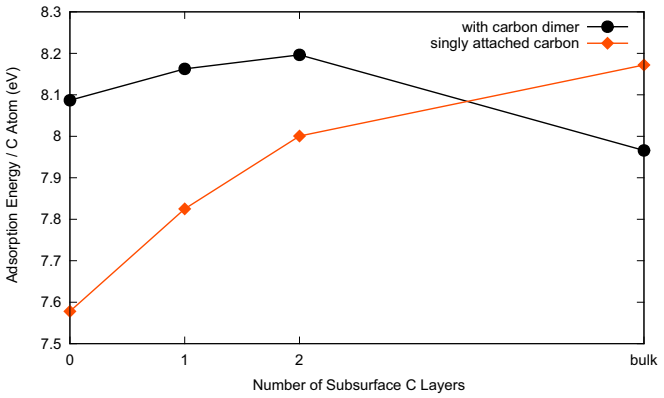

FIG. 11. (Color online) Calculated adsorption energies per carbon atom on Mo(110) with increasing number of subsurface carbon layers for 3/8 surface coverage. See Fig. 5 for arrangements of the surface carbon atoms.

227.85 eV for the monolayer carbide and 227.96 eV for the surface carbide on top of bulk carbide. The binding energy of the bulk Mo_2C peak is 228.23 eV.

To obtain additional information, we measured Mo $3d_{5/2}$ and C 1s spectra of the bulk carbide at different photon energies; the spectra, including the fits, are shown in Fig. S11 in the Supplemental Material [39]. Figure 10(a) shows the analysis for the two peaks of the Mo $3d_{5/2}$ region. As expected, the surface contribution decreases with increasing kinetic energy, while the bulk contribution clearly increases. In the C 1s region [Fig. 10(b)], the two main peaks exhibit nearly the same intensity with a surface-to-bulk ratio of 10:9 at $h\nu = 380$ eV (∼100 eV kinetic energy). With increasing photon energy, this ratio strongly decreases to ∼3:10 at 680 eV (∼400 eV kinetic energy), and the defect peak vanishes. This supports our assignment of the peak at 283.43 eV to bulk Mo_2C, the peak at 282.99 eV to the surface carbide on top of the bulk carbide, and the peak at 282.4 eV to surface defects.

The surface carbon peak at 282.89 eV in the C 1s region corresponds to 0.55 ± 0.06 ML. Assuming an IMFP of the photoelectrons of 4.5 Å in Mo at ∼100 eV kinetic energy [41] and similar carbon amounts in every equally thick carbide layer gives a ratio of roughly 1:1 between a nondamped carbon surface layer compared to the damped bulk signal. If we postulate a carbon-terminated surface, this is in agreement with the measured data. While being aware of the systematic errors involved in both peak fitting and due to our simple model, we reason that the surface coverage is roughly 0.5 ML, as also determined from our calibration. Please note that the coverage of the surface peak slightly increased from 1200 to 140 K [see Fig. 9(a)]. We attribute this to different solubility of carbon in Mo at lower temperatures, leading to diffusion to the surface.

Interestingly, and contrary to the single layer C/Mo(110), DFT calculations predict that single carbon atoms on Mo_2C are more stable than carbon dimers. In Fig. 11, the adsorption energy per carbon atom of dimers and single carbon atoms, respectively, depending on the number of carburized subsurface layers, is shown. Whereas for the "clean" Mo(110) surface the dimers are clearly energetically favored, the preference becomes smaller with the number of subsurface carbon layers. Finally, for the surface of bulk Mo_2C adsorption, geometries with single carbon atoms are more stable. An explanation for this behavior may be that a geometric change of the surface occurs with increasing carburization of the lower layers: the distorted hexagonal (orthorhombic) surface of Mo(110) gradually turns into the quasihexagonal surface of Mo_2C. Thus, the preferred adsorption sites for the carbon dimers (lengthy rhombi, accommodating the carbon dimers) vanish, leading to a destabilization of the carbon dimers on the Mo_2C surface relative to single carbon atoms, which are located at threefold hollow sites.

Next, we discuss the removal of the bulk carbide by exposure to oxygen from the supersonic molecular beam at pressures from 1.8×10^{-6} to 2.7×10^{-6} mbar at 1200 K. The corresponding Mo $3d_{5/2}$ and C 1s spectra are shown Figs. 8(c) and 8(d), respectively. Note that slightly different peak shapes between the last spectra in the carburization experiment in Figs. 8(a) and 8(b), and the first spectra in the oxidation experiment are due to diffusion from the surface near region to the bulk after the ethylene beam was switched off (see above). Upon oxygen exposure, we find an immediate decrease of the bulk peaks in the Mo $3d_{5/2}$ and C 1s regions, see Figs. 8(c) and 8(d). The C 1s surface carbide peak also decreases by ∼20% up to 3000 L, while the Mo SCLS peak appears and increases to ∼30% of its maximum value for the clean surface. Interestingly, between 3000 and 5000 L, we observe a flattening of all curves in the quantitative analysis in Figs. 9(e) and 9(f), and the Mo $3d_{5/2}$ spectra show only minor changes in the ratio of surface and bulk peaks. This behavior is attributed to continuous diffusion of carbon to the

surface, from deeper layers beyond the information depth of our experiment. Above this exposure, we observe a shift of the C 1*s* surface carbide to lower binding energy, to the value of 282.73 eV found for the monolayer carbide (see above), and a fast decrease of the total area. At the same time, in the Mo $3d_{5/2}$ region a strong increase of the Mo SCLS peak at 227.64 eV is found. At ∼6000 L, the C 1*s* signal has completely vanished, and the Mo SCLS peak has reached its maximum intensity, indicating that at this exposure the Mo(110) surface is nearly clean. Finally, the Mo SCLS peak strongly decreases, and at the same time the oxygen-derived peaks at 227.78 and 228.16 eV start to grow.

Overall, the observed behavior is in line with the proposed carbon diffusion into the bulk upon carburization. Upon exposure to oxygen, the bulk has to be depleted of carbon in order to finally be able to oxidize the surface. Under the applied conditions, carbon diffusion from the bulk to the surface seems to be the rate-limiting step of this process.

C. Monolayer carbide preparation and oxidative removal on Mo(100)

In order to compare the behavior during carburization of different crystal facets, we prepared a monolayer carbide also on the Mo(100) surface at similar conditions as for Mo(110); the corresponding data are shown in Fig. 12. We start our experiment from a Mo(100) surface that is precovered with ∼0.1 ML of oxygen. Prior to exposure to ethylene (0 L), the Mo $3d_{5/2}$ region displays the Mo bulk peak at 227.90 eV and a weak Mo SCLS peak at 227.50 eV. The preadsorbed oxygen leads to a broad contribution at 228.25 eV and a second peak at 228.00 eV. As expected, no peaks are found in the C 1*s* region.

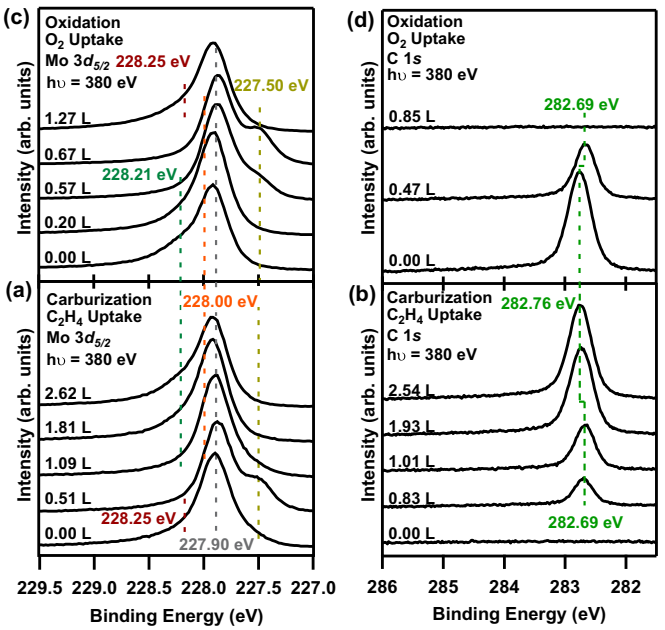

FIG. 12. (Color online) Selected XP spectra of the monolayer carbide preparation on Mo(100) at different doses of ethylene both in the (a) Mo $3d_{5/2}$ and the (b) C 1*s* core levels. (c), (d) Respective spectra of the subsequent oxidation are presented (T_S = 1200 K, $h\nu$ = 380 eV).

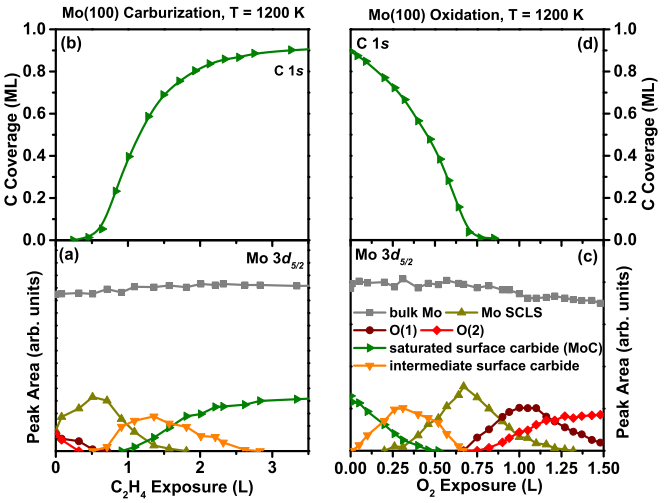

FIG. 13. (Color online) Quantitative analysis of the monolayer carbide preparation on Mo(100) both in the (a) Mo $3d_{5/2}$ and (b) the C 1*s* core levels. (c), (d) Analysis of the subsequent oxidation is presented (T_S = 1200 K, $h\nu$ = 380 eV).

Upon exposure to 1.4×10^{-8} mbar ethylene, we observe an increase of the Mo SCLS peak at the cost of the oxygen-derived peak, as evident from the quantitative analysis in Fig. 13(a). The Mo $3d_{5/2}$ spectrum at 0.51 L in Fig. 12(a) represents an almost clean surface. Above this exposure, we find the increase of a sharp C 1*s* peak at 282.69 eV, accompanied by the decrease of the Mo SCLS peak in the Mo $3d_{5/2}$ region and by the appearance of a peak at 228.0 eV (intermediate surface carbide, orange in Fig. 13), which we assign to the partially covered (low-coordinated) Mo surface atoms. Above 1 L, we find a new Mo $3d_{5/2}$ peak at 228.21 eV, which is assigned to saturated monolayer carbide (MoC) on the surface (green in Fig. 13). This contribution is close to the binding energy of the oxide contribution, but as no oxygen is left on the surface, it is unambiguously assigned to the carbide. Above 3 L, this peak saturates, while the intermediate surface carbide peak vanishes completely. During the formation of the MoC monolayer carbide, the C 1*s* peak shifts to slightly higher binding energy of 282.76 eV. The carburization experiment was performed up to an exposure to 4.2 L; since above 3.5 L no further changes occurred, only this exposure range is shown in Fig. 13(a).

From the literature [27,36,42], we know that an intermediate $c(2 \times 2)$ structure exists for a coverage of 0.5 ML of carbon, which is followed by the $p(1 \times 1)$ structure that is found at saturation. In the $c(2 \times 2)$ structure, the Mo atoms are coordinated to only two carbon atoms as compared to four atoms in the (1×1) structure. This could explain the observation of the intermediate Mo $3d_{5/2}$ surface carbide peak (in the presence of the lower coordinated carbon atoms) at ∼0.5 ML and the saturated monolayer carbide (with the higher coordinated carbon atoms) at 1.0 ML in the Mo $3d_{5/2}$ spectra.

To obtain better insight, we also measured the spectra of the saturated monolayer carbide at temperatures of 140 K; this monolayer carbide displays a (1×1) pattern in LEED. The C 1*s* spectrum in Fig. 14(b) shows a sharp peak at 282.88 eV, along with a small peak at 282.35 eV, which is

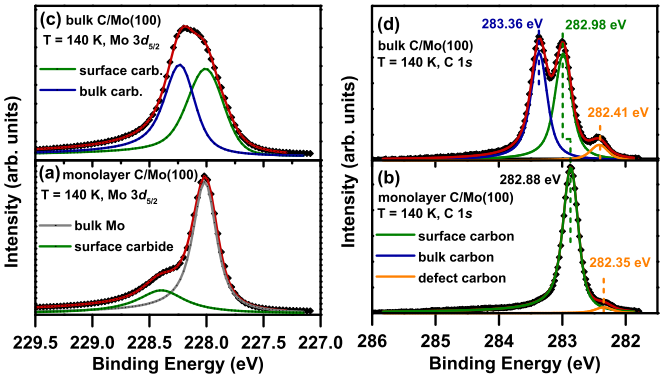

FIG. 14. (Color online) Comparison between the monolayer (a) and (b) and bulk (c) and (d) carbide overlayers of C/Mo(100) at low temperatures for the (a) and (c) Mo $3d_{5/2}$ core level and (b) and (d) C 1*s* core level ($T < 140$ K, $h\nu = 380$ eV).

attributed to defects, in analogy to the contribution found for the bulk carbide on Mo(110) (see above). The main peak corresponds to a carbon coverage of 0.95 ± 0.10 ML. In the Mo $3d_{5/2}$ region in Fig. 14(a), we find the metallic Mo bulk peak at 228.00 eV and the monolayer carbide peak at 228.42 eV. The small binding energy differences as compared to Fig. 12 are again attributed to the applied heating current and/or thermal broadening at the elevated temperature. To verify the identification as bulk and surface peaks, we varied the photon energy for the Mo $3d_{5/2}$ spectra. Figure 15 shows the relative peak intensities versus kinetic energy of the photoelectrons. The continuous decrease of the monolayer carbide peak and increase of the Mo bulk peak with increasing kinetic energy confirm our assignment. These results are in agreement with a structure deduced from LEED-IV analysis [36], where all hollow sites of the (100) bcc facet are occupied by carbon, leading to a nominal coverage of 1 ML.

Computations of the Mo(100) monolayer carbide with 0.5 and 1 ML support these assignments. From the structural viewport, we find that on a Mo(100) surface the carbon atoms adsorb at the fourfold hollow sites with an even higher adsorption energy than on Mo(110): 9.15 eV (0.5 ML) and 8.56 eV (1 ML), respectively. The calculated SCLS show that the SCLS for 3*d* Mo becomes more positive with an increasing

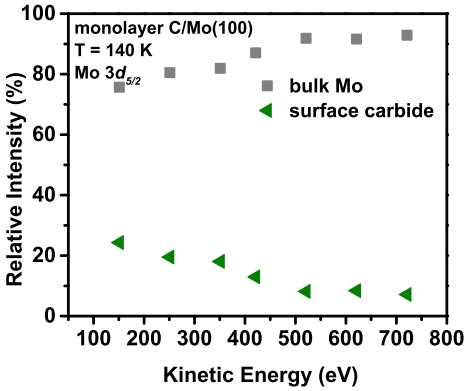

FIG. 15. (Color online) Relative ratios of Mo $3d_{5/2}$ core level peaks of the monolayer carbide $p(1 \times 1)$−C/Mo(100) for different kinetic energies of the photoelectrons.

carbon attachment on the surface. The 3*d* Mo SCLS of the clean Mo(100) surface is calculated at −0.93 eV (which is a significantly larger shift than the measured one of −0.40 eV). For 0.5 ML carbon on the surface, the calculated SCLS is reduced to −0.16 eV, and for 1 ML we find a theoretical value of +0.33 eV. This means that the order of the calculated core level shift is qualitatively in agreement with experiment, but quantitatively a significantly stronger shift is calculated.

Next we discuss the removal of the monolayer carbide on Mo(100) by exposure to 3.7×10^{-9} mbar O_2 at 1200 K. In Figs. 12(c) and 12(d), the Mo $3d_{5/2}$ and C 1*s* spectra are presented, respectively. The starting point of this experiment (at 0 L) is the end point of the carburization experiment (at 4.2 L). Upon oxygen exposure, the monolayer carbide (MoC) peak at 228.21 eV in Fig. 13(c) decreases, and at the same time, the intermediate surface carbide peak at 228.0 eV increases, indicating the partial removal of carbon from the surface. This contribution reaches its maximum value at approximately 0.3 L, followed by its decrease, while the Mo SCLS peak at 227.50 eV increases. Simultaneously, the C 1*s* peak decreases, shifts to lower binding energies [282.69 eV in Fig. 12(d)], and finally vanishes around ∼0.7 L [Fig. 13(d)]. At this exposure, the Mo SCLS peak has reached its maximum, which indicates a clean surface. For higher oxygen exposures, the Mo SCLS peak decreases, and the oxygen-induced Mo peaks starts to grow at 228.0 and 228.25 eV, respectively. An important difference to the oxidation of the monolayer carbide on Mo(110) is that we do not observe the slow onset of the carbide removal, which we attributed to initial diffusion of carbon from the bulk to the surface. Together with the observation that the bulk carbide at 1200 K on Mo(100) grows very slowly, we conclude that nearly any carbon diffuses to the bulk during carburization at this temperature. Consequently, only carbon on the surface has to be removed during oxidation, and only a small amount of O_2 (∼0.7 L) is needed to oxidize all the carbon in the system. From these findings, we conclude that the saturated monolayer carbide is stable and that no diffusion from the surface to the bulk or vice versa occurs at 1200 K, which also implies that nearly any ethylene is dissociating on the monolayer carbide surface.

D. Bulk carbide preparation and oxidation on Mo(100)

The next goal was the preparation of a bulk carbide on Mo(100). We started with conditions where on Mo(110) a bulk carbide forms, that is, high exposures to ethylene at 1200 K. However, upon expose of the monolayer carbide on Mo(100) to high ethylene doses of ∼2000 L, we only observe a very slow growth of a bulk Mo_2C peak (not shown), indicating a very low reaction rate of ethylene at 1200 K after saturation of the monolayer carbide, in line with the literature [43].

Consequently, we followed a different route, which consists of cycles of ethylene exposure at 900 K followed by flashing to 1300 K [23,24]. In Fig. 16(a), C 1*s* spectra collected during exposure of a Mo(100) surface to ethylene at 900 K at a pressure of 2.8×10^{-7} mbar are shown. The experiment starts with a surface precovered with a very small amount of carbon (∼0.05 ML) that remained on the surface after the cleaning procedure. At low exposures, we observe a peak at 282.70 eV, very similar to that found for the monolayer carbide prepared at 1200 K (see above). Above 150 L, this peak shifts to higher binding energy and develops a high energy

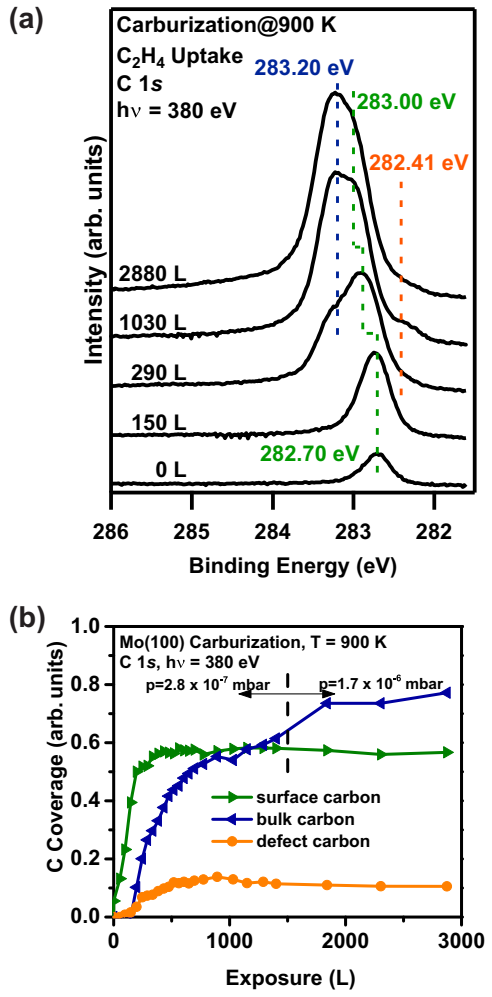

FIG. 16. (Color online) (a) Selected XP spectra of the thick carbide preparation on Mo(100) at different doses of ethylene in the C 1*s* core level. Note that the experiment started with only a low amount of carbon preadsorbed; (b) quantitative analysis of the respective experiment ($T_S = 900\,\mathrm{K}$, $h\nu = 380\,\mathrm{eV}$).

shoulder, and finally a second peak at 283.2 eV appears. These peaks are assigned to the surface carbide layer and the bulk carbide, respectively, similar to the behavior on Mo(110) at 1200 K. The additional small peak 282.41 eV is due to surface defects, similar as for the bulk carbide on Mo(110). From the quantitative analysis in Fig. 16(b), it is evident that the surface carbide peak saturates at ∼200 L, while the bulk peak continues to grow slowly. At 1000 L, surface and bulk contributions show approximately the same total intensity, and the defect peak has saturated. To speed up the process, we increased the pressure to 1.7×10^{-6} mbar above 1500 L. The resulting stronger increase of the bulk peak points to a pressure dependence of the growth process. It is due to the slower diffusion of carbon into the bulk compared to our other experiments at 1200 K.

The final step of the carburization process is a flash to 1300 K, after which no further ethylene is supplied. Notably, after this heating step, the surface and bulk peaks in the C 1*s* spectra are significantly more narrow than in Fig. 16 (see Fig. 17 for comparison), which is attributed to a more defined

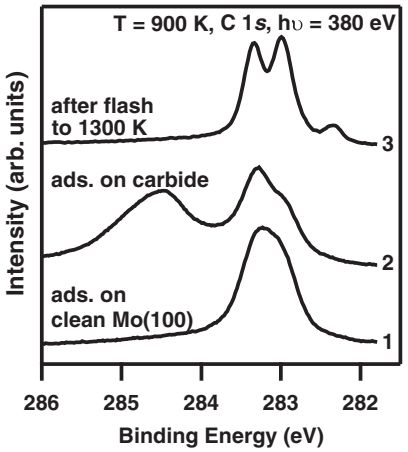

FIG. 17. XP spectra in the C 1*s* core level showing the difference of the carburization process with and without flashes to 1300 K ($T = 900\,\mathrm{K}$, $h\nu = 380\,\mathrm{eV}$). See the text for details.

carbide state. The resulting Mo $3d_{5/2}$ and C 1*s* spectra after cooling to below 140 K in vacuum are shown in Figs. 14(c) and 14(d).

The spectra in Fig. 17 after adsorption at 900 K (1) and after flash to 1300 K (3) reflect carburization of a more or less clean crystal. Upon carburization of a Mo(100) surface covered with the saturated monolayer carbide at 900 K, we find a very different behavior, namely the growth of a new peak at ∼284.5 eV [see spectrum (2) in Fig. 17]. We believe that the saturated monolayer carbide (MoC) prevents diffusion from the surface into the bulk; thus, upon ethylene exposure at 900 K, one instead observes the formation of a graphitelike layer on the surface. This graphite layer only vanishes when annealing to temperatures above 1050 K [spectrum (3) in Fig. 17] since diffusion into the bulk is possible at this elevated temperature.

The spectrum of the bulk carbide on Mo(100) in Fig. 14 shows strong similarities with the bulk carbide of C/Mo(110) (Fig. 3). In the C 1*s* region in Fig. 14(d), we also find three peaks: a surface carbide peak at 282.98 eV, a defect peak at 282.41 eV, and a bulk carbide peak at 283.36 eV. The surface carbide peak has the same binding energy as for Mo(110), and the bulk carbide peak and the defect peak are shifted by 0.05 and 0.06 eV, respectively [cf. Fig. 3(d)]. In the Mo $3d_{5/2}$ region in Fig. 14(c), we observe two peaks due to bulk Mo_2C (228.23 eV) and the surface carbide layer (228.00 eV). These peak assignments are supported by Mo $3d_{5/2}$ spectra collected at different photon energies (see Fig. S12 [39]).

In order to check reproducibility of the carburization process, we performed several sputter-anneal cycles and numerous carburization experiments, all showing the same surface and bulk peak positions. Only the defect peak in the C 1*s* region varies in intensity from preparation to preparation, thus supporting its assignment to defect sites on the surface.

When comparing the Mo $3d_{5/2}$ spectra on Mo(110) and Mo(100) in Figs. 3 and 14, respectively, we find significant differences between the saturated carbide monolayers on the two surfaces. On Mo(110), the binding energy of the monolayer carbide (227.85 eV) is smaller than that of the Mo bulk (228.0 eV), whereas on Mo(100) the binding energy (228.42 eV) is larger. This difference is mainly attributed to the

higher coordination of Mo surface atoms to carbon atoms at the higher carbon coverage of 1.0 ML on Mo(100), as compared to 0.5 ML on Mo(110). Interestingly, the bulk carbides show great similarities for the two substrates. In particular, both show a surface carbide peak at ∼228.00 eV. Only the relative intensity of the two peaks is different. This raises the question as to whether the structure of the unit cell directly on the surface is still close to that of the monolayer carbide. Our coverage calibration for Mo(100) yields a C coverage of ∼0.7 ML for both the surface and bulk carbon peaks of the bulk carbide. If the bulk stoichiometry holds to be Mo 2:1 C, the bulk carbide peak is expected to be of the same intensity as for the bulk Mo(110) carbide. If the surface faceted to a (110) surface at the top, a coverage of 0.5 ML would result, which agrees better with the known stoichiometry of bulk Mo_2C [8]. Faceting would also explain the different relative intensities of surface and bulk peak in the Mo $3d_{5/2}$ core level. In LEED we find a diffusive 1×1 structure for the bulk carbide and fast outward moving spots upon variation of the electron kinetic energy [44,45], and also from the XPS point of view, it looks as if the carburization at 900 K and subsequent flashing to 1300 K on Mo(100) leads to massive reconstruction, that is, faceting towards the structure of the bulk C/Mo(110) carbide. This is also supported by the structures found in SEM (see Fig. S13 [39]).

III. CONCLUSION

We performed a combined *in situ* XPS study and DFT investigation of the formation of carbide-modified surfaces on Mo(110) and Mo(100).

On Mo(110), we followed the preparation of monolayer and bulk carbides by continuously recording Mo $3d_{5/2}$ and C 1*s* XP spectra during exposure to ethylene at 1200 K, from zero carbon content up to saturation. Notably, despite the high temperature, the spectra show narrow peaks, and the SCLSs in the Mo $3d_{5/2}$ spectra can be used to identify contributions originating from the clean surface as well as Mo atoms in contact to carbon or oxygen. In line with literature [4,12,32,33], our experimental results and the calculations of the bulk carbide on Mo(110) indicate a very similar surface structure compared to the carbon-terminated (001) surface of orthorhombic bulk Mo_2C. Single carbon atoms are found in the threefold hollow sites of the underlying quasihexagonal Mo lattice. Our calibration from XPS yields a coverage of 0.55 ± 0.06 ML surface carbon atoms per Mo atom, in excellent agreement with the nominal value. For the monolayer carbide on Mo(110), however, we find a lower surface coverage of 0.43 ± 0.06 ML. Our calculations show that this surface exhibits a different structure due to carbon dimer formation in the nearest neighbor long-bridge sites. For the (4×4) LEED pattern, we propose a surface structure that has a coverage of $3/8$ ML $= 0.375$ ML, which within the margin of error is in line with the experimentally derived value.

On Mo(100), we prepared a well-defined monolayer carbide at 1200 K, with a coverage of 0.95 ± 0.10 ML, which is in excellent agreement with the (1×1) pattern observed in LEED. Our calculations indicate that carbon occupies the fourfold symmetric hollow sites of the (100) facet, as reported previously [36]. The bulk carbide on Mo(100) was prepared by ethylene cracking at 900 K and flashes to 1300 K. This preparation method of the bulk carbide on Mo(100) most probably leads to faceting of the surface, yielding a bulk C/Mo(110) carbidelike structure.

For both surfaces, the removal of the carbide by exposure to oxygen at elevated temperatures was also followed in detail.

IV. EXPERIMENTAL

The HR-XPS experiments were performed at the beamline U49/2-PGM1 of the synchrotron facility BESSY II in Berlin using a transportable UHV setup [46]. The preparation chamber houses typical surface-science instruments such as electron beam evaporators, a sputter gun, a two-grid LEED optics, and dosing facilities. The analysis chamber with a base pressure of 2×10^{-10} mbar is equipped with an electron energy analyzer (EA 125 HR U7) and a QMS. Furthermore, a three-stage supersonic molecular beam chamber is directly connected to this chamber, generating a collimated monochromatic molecular beam that impinges on the sample at 45°. This enables us to dose gases at relatively high pressures (up to 1×10^{-5} mbar) at the sample, while the background pressure never exceeds values above 5×10^{-8} mbar. The sample can be cooled using liquid nitrogen to approximately 120 K, and temperatures up to 1400 K can be reached using resistive heating. During the experiments, XP spectra were obtained continuously with typically 10 s per spectrum. The spectra at a photon energy of 380 eV (650 eV) were acquired at a resolution of 180 meV (240 meV) at a photoelectron emission angle of 0° with respect to the sample normal. The binding energy scale has been calibrated by the Fermi edge measured both at low temperature and during resistive heating.

The Mo(110) and Mo(100) crystals (MaTecK, 99.99%) were spot-welded to Ta wires, and thermocouples (type K) were attached directly to the sample. Ar^+ bombardment (1 kV, 4×10^{-6} mbar) was used for cleaning, followed by annealing in vacuum to 1300 K and subsequent checks by XPS prior to the experiments. Dioxygen gas (5.0) was purchased from Westfalen AG, and ethylene (3.5) was purchased from Air Liquide Germany GmbH.

The carbon coverages were calibrated by comparison to the known $c(4 \times 2)$ CO superstructure on Pt(111) [47]. The oxygen coverages (uncertainty ∼20%) were calibrated using a separate adsorption experiment of CO on the monolayer carbide of Mo(110) (data not shown). For fitting, we subtracted the background and used Doniach-Sunjic [48] functions convoluted with a Gaussian to represent the peak shape.

Scanning electron microscopy was performed in a UHV setup (Multiscanlab, Omicron Nanotechnology). The SEM uses an electron column (Leo Gemini) that allows SEM at a resolution down to 3 nm. For the images, the electron energy was 15 keV; for details, see, e.g., Ref. [49].

V. COMPUTATIONAL METHODS

Density-functional theory calculations were performed with the Vienna *Ab initio* simulation package (VASP) using the projector-augmented wave (PAW) approach [50] and a plane-wave basis set with a cutoff energy of 430 eV. The exchange-correlation functional by Perdew, Burke, and Ernzerhof (PBE) [51] was applied. The rectangular

C/Mo(110) cells and C/Mo(100) surfaces were modeled by slabs of six Mo layers separated by a vacuum layer of approximately 18 Å. The PAW approach was used to treat 28 electrons $[1s^2\,2s^2\,2p^6\,3s^2\,3p^6\,3d^{10}]$ in the core for Mo and two electrons $[1s^2]$ for C. The three lowest molybdenum layers of the slab were kept fixed at the bulk geometry with a bcc lattice constant of 3.163 Å, which was determined by structural optimization of the Mo bulk. In case of the single layer (4×4) C/Mo surfaces, a somewhat simpler model was applied by reducing the number of Mo layers to four (keeping the lower two layers fixed), setting the vacuum distance to approximately 10 Å, and using a PAW pseudopotential for Mo with 36 electrons $[1s^2\,2s^2\,2p^6\,3s^2\,3p^6\,3d^{10}\,4s^2\,4p^6]$ in the core. To check the accuracy of this reduced model, the adsorption energy per carbon atom on Mo(110) with 1/2 ML, which can be modeled using a (2×2) supercell, was calculated using both computational setups. Since both setups yield the same adsorption energy up to 7 meV, we consider both models to be reliable.

The first Brillouin zone was sampled by Monkhorst-Pack k-point grids [52] with $11 \times 11 \times 1$ k-points for rectangular Mo(110) surfaces, $7 \times 7 \times 1$ k-points for (4×4) Mo(100) surfaces, and $18 \times 18 \times 1$ k-points for (1×1) Mo(100) surfaces k-points (here the Monkhorst-Pack grid was shifted to contain the Γ point). Methfessel-Paxton smearing [53] of order 1 and a width of $\sigma = 0.2$ eV was applied throughout. For analysis, the extrapolated energies for $\sigma \to 0$ were used.

The convergence criterion for the wave function was 10^{-6} eV, and for geometry relaxations the maximal allowed Cartesian force component was 10^{-3} eV/Å. All calculations are non-spin-polarized, which was justified by some spin polarized single point calculations for different geometries.

Core level binding energies ε_{CL} were computed by removing one electron from the core orbital of interest and adding one electron to the Fermi level. The response of the valence electrons to the core hole is taken into account by subsequent electronic relaxation, i.e., by carrying out a self-consistent calculation on this electronic configuration (final state approximation). The core level binding energy ε_{CL} is then approximated as $\varepsilon_{CL} = \varepsilon_C - \varepsilon_F$, where ε_C is the absolute core orbital energy and ε_F the Fermi level. Since the core states are kept frozen within the PAW approach, screening effects of the core electrons are neglected. Therefore, absolute values of the core level energies will have substantial errors compared to experiment that can be, however, expected to cancel approximately if core level energy differences, i.e., shifts, are compared. Moreover, the generated hole is always spherical, i.e., multipole splittings are not available. The addition of the excited electron to the Fermi level is a further approximation, which is required to retain a charge neutral unit cell. To check the quality of this approximation, we actually removed the electron and added instead a negative background charge in some cases. We found that the results are practically the same for both methods.

Surface core level shifts of the different surface Mo species were calculated as the difference between the core level binding energy of a bulk Mo atom and the considered surface Mo atom.

Constant current STM images are simulated within the Tersoff-Hamann model [54,55]. The applied bias voltage was −372 mV, corresponding to the experimental setting by Yu *et al.* [28].

To determine adsorption energies per carbon atom, the energy of a single carbon atom was computed in the cell of the (4×4) Mo(110) surface (spin polarized, one k-point).

[1] S. T. Oyama, *The Chemistry of Transition Metal Carbides and Nitrides* (Blackie A&P, Glasgow, 1996).
[2] L. I. Johansson, Surf. Sci. Rep. **21**, 177 (1995).
[3] J. G. Chen, Chem. Rev. **96**, 1477 (1996).
[4] H. H. Hwu and J. G. Chen, Chem. Rev. **105**, 185 (2005).
[5] R. B. Levy and M. Boudart, Science **181**, 547 (1973).
[6] W. F. Chen, J. T. Muckerman, and E. Fujita, Chem. Commun. **49**, 8896 (2013).
[7] A. L. Stottlemyer, T. G. Kelly, Q. Meng, and J. G. Chen, Surf. Sci. Rep. **67**, 201 (2012).
[8] E. Parthé and V. Sadogopan, Acta Crystallogr. **16**, 202 (1963).
[9] A. N. Christensen, Acta Chem. Scand. **31a**, 509 (1977).
[10] T. P. St. Clair, S. T. Oyama, D. F. Cox, S. Otani, Y. Ishizawa, R. L. Lo, K. I. Fukui, and Y. Iwasawa, Surf. Sci. **426**, 187 (1999).
[11] R. L. Lo, K. I. Fukui, S. Otani, and Y. Iwasawa, Surf. Sci. **440**, L857 (1999).
[12] R. L. Lo, K. I. Fukui, S. Otani, S. T. Oyama, and Y. Iwasawa, Jpn. J. Appl. Phys. **38**, 3813 (1999).
[13] T. Wang, Q. Luo, Y. W. Li, J. Wang, M. Beller, and H. Jiao, Appl. Catal. A-Gen. **478**, 146 (2014).
[14] J. R. D. S. Politi, F. Viñes, J. A. Rodriguez, and F. Illas, Phys. Chem. Chem. Phys. **15**, 12617 (2013)
[15] T. Wang, Y. W. Li, J. Wang, M. Beller, and H. Jiao, J. Phys. Chem. C **118**, 3162 (2014).
[16] X. R. Shi, S. G. Wang, H. Wang, C. M. Deng, Z. F. Qin, and J. G. Wang, Surf. Sci. **603**, 852 (2009).
[17] X. R. Shi, J. G. Wang, and K. Hermann, J. Phys. Chem. C **114**, 13630 (2010).
[18] X. R. Shi, S. G. Wang, J. Hu, Z. F. Qin, and J. G. Wang, Surf. Sci. **606**, 1187 (2012).
[19] X. Liu, A. Tkalych, B. Zhou, A. M. Köster, and D. R. Salahub, J. Phys. Chem. C **117**, 7069 (2013).
[20] C. De Oliveira, D. R. Salahub, H. A. De Abreu, and H. A. Duarte, J. Phys. Chem. C **118**, 25517 (2014).
[21] M. Bode, R. Pascal, and R. Wiesendanger, Surf. Sci. **344**, 185 (1995).
[22] P. F. Lyman and D. R. Mullins, Phys. Rev. B **51**, 13623 (1995).
[23] T. Schöberl, Surf. Sci. **327**, 285 (1995).
[24] L. Ovari, J. Kiss, A. P. Farkas, and F. Solymosi, Surf. Sci. **566**, 1082 (2004).
[25] M. B. Young and A. J. Slavin, Surf. Sci. **245**, 56 (1991).
[26] B. Frühberger and J. G. Chen, Surf. Sci. **342**, 38 (1995).
[27] C. Guillot, R. Riwan, and J. Lecante, Surf. Sci. **59**, 581 (1976).
[28] D. W. Yu, Y. H. Wu, R. B. Lin, and R. L. Lo, J. Phys.: Condens. Matter **20**, 135004 (2008).
[29] J. W. He, W. K. Kuhn, and D. W. Goodman, Surf. Sci. **262**, 351 (1992).

[30] C. L. Roe and K. H. Schulz, J. Vac. Sci. Technol. A **16**, 1066 (1998).
[31] B. Frühberger and J. G. Chen, JACS **118**, 11599 (1996).
[32] J. R. Kitchin, Ph.D. Thesis, University of Delaware, Newark, Delaware, 2004.
[33] B. Frühberger, J. G. Chen, J. Eng, and B. E. Bent, J. Vac. Sci. Technol. A **14**, 1475 (1996).
[34] A. C. Lausche, J. A. Schaidle, and L. T. Thompson, Appl. Catal. A-Gen. **401**, 29 (2011).
[35] D. Jentz, S. Rizzi, A. Barbieri, D. Kelly, M. A. Van Hove, and G. A. Somorjai, Surf. Sci. **329**, 14 (1995).
[36] M. Kottcke, R. Döll, W. Weiß, F. Seiferlein, W. Arabczyk, L. Hammer, and K. Heinz, Surf. Sci. **352**, 592 (1996).
[37] S. H. Overbury and P. C. Stair, J. Vac. Sci. Technol. A **1**, 1055 (1983).
[38] M. Smedh, S. F. Diaz, and C. T. Campbell, Phys. Rev. B **67**, 205401 (2003).
[39] See Supplemental Material at http://link.aps.org/supplemental/10.1103/PhysRevB.92.014114 for further experiments, calculations and details of our fitting procedure.
[40] E. Lundgren, U. Johansson, R. Nyholm, and J. N. Andersen, Phys. Rev. B **48**, 5525 (1993).
[41] S. Tanuma, C. J. Powell, and D. R. Penn, Surf. Interface Anal. **35**, 268 (2003).
[42] L. Hammer, M. Kottcke, K. Heinz, K. Müller, and D. M. Zehner, Surf. Rev. Lett. **03**, 1701 (1996).
[43] E. I. Ko and R. J. Madix, Surf. Sci. **109**, 221 (1981).
[44] A. U. M. Rae, Surf. Sci. **4**, 247 (1966).
[45] L. G. Feinstein and M. S. Macrakis, Surf. Sci. **18**, 277 (1969).
[46] R. Denecke, M. Kinne, C. M. Whelan, and H.-P. Steinrück, Surf. Rev. Lett. **09**, 797 (2002).
[47] J. S. McEwen, S. H. Payne, H. J. Kreuzer, M. Kinne, R. Denecke, and H. P. Steinrück, Surf. Sci. **545**, 47 (2003).
[48] S. Doniach and M. Sunjic, J. Phys. C **3**, 285 (1970).
[49] M. Schirmer, M. M. Walz, C. Papp, F. Kronast, A. X. Gray, B. Balke, S. Cramm, C. S. Fadley, H. P. Steinrück, and H. Marbach, Nanotechnology **22**, 475304 (2011).
[50] G. Kresse and J. Furthmüller, Comp. Mater. Sci. **6**, 15 (1996).
[51] J. P. Perdew, K. Burke, and M. Ernzerhof, Phys. Rev. Lett. **77**, 3865 (1996).
[52] H. J. Monkhorst and J. D. Pack, Phys. Rev. B **13**, 5188 (1976).
[53] M. Methfessel and A. T. Paxton, Phys. Rev. B **40**, 3616 (1989).
[54] J. Tersoff and D. R. Hamann, Phys. Rev. Lett. **50**, 1998 (1983).
[55] J. Tersoff and D. R. Hamann, Phys. Rev. B **31**, 805 (1985).